
Neutron-Induced Nucleation Inside Bubble Chambers Using Freon 115 as the Active Medium

Introduction

The vast majority of controlled fusion experiments worldwide involve deuterium–tritium (DT) or deuterium–deuterium (DD) mixtures.¹ Nuclear diagnostics provide a direct measurement of the DD or DT fusion burn within a compressed inertial confinement fusion (ICF) target.² These diagnostics are used to infer the fuel areal density, neutron yield, fuel-ion temperature, and bang time.² Neutrons are a primary fusion-reaction product that can provide an image of the fusion burn region. Neutron imaging (NI) can be used to determine failure modes of ICF ignition capsules, such as poor implosion symmetry or improper laser pulse shaping.^{3,4} NI has been used on OMEGA⁵ to measure the core symmetry of gas-filled plastic shells and cryogenic target implosions.⁶ NI systems use extended pinholes or penumbral apertures (with annular apertures as a particular case) to capture images on a neutron-sensitive detector.⁴ They are sensitive to both alignment and fabrication errors of the apertures used.⁷

A neutron image provides a direct measurement of the spatial extent of the fusion burn area for an ICF implosion, drawn from the physical characteristics of the neutrons that exit the plasma core as primary or secondary products of the fusion reactions.⁴ The core image is obtained by placing an appropriate aperture in front of a spatially sensitive neutron detector. The apertures are typically coded.⁴ The neutrons are detected by a plastic scintillator⁶ array or a bubble chamber.⁸

In NI systems, the coded image must be deconvolved to produce an accurate representation of the neutron source. This process requires precise knowledge of the aperture point-spread function (PSF) and the flat-field response of the imaging detector.³ Both pinhole and penumbral apertures are used.⁷ For both pinholes and penumbral apertures, uncertainties in the exact shape (caused by finite fabrication tolerances) lead to errors in the reconstructed image because of uncertainties in the calculated PSF. A computational study⁷ previously investigated the influences of various parameters from the NI system on the quality of the reconstructed image.

The required spatial resolution for an imaging system can be determined from numerical simulations.² A resolution of about 10 μm appears to provide sufficient information to validate implosion models, but a resolution of 5 μm may be necessary to see details in the implosion structure.² Previous studies⁸ have already shown that bubble chambers have the potential to obtain higher-resolution images of the targets for a shorter source–target distance than typical scintillator arrays and could be used for the very high neutron yields ($\geq 10^{16}$) expected to be measured at the National Ignition Facility (NIF).

This article discusses the mechanism of neutron-induced bubble formation inside Freon 115 and the influence of the critical radius size on the neutron detection sensitivity. Two forthcoming publications will focus on the design of the liquid Freon bubble chamber used on OMEGA and the data recorded with the detector, respectively.^{9,10}

Interactions of Neutrons with Freon 115— A Simplified Model

Freon 115 (chloropentafluoroethane, $\text{C}_2\text{F}_5\text{Cl}$) has been used as the active medium in bubble chambers for high-energy-physics experiments at the European Organization for Nuclear Research (CERN) since the early 1980s.¹¹ It is nonflammable, inexpensive, safe to operate, and easy to store in compressed gas tanks. A Freon 115 bubble chamber does not need cryogenic cooling and can be operated at around 50°C.

1. Thermodynamic Conditions for Bubble Formation

A bubble chamber is initially pressurized with its active medium in a liquid state. Several milliseconds before the incident particles enter the chamber, the pressure is quickly decreased and the liquid enters a superheated, metastable phase. The temperature becomes higher than its standard boiling point, without actually boiling. Deposition of small quantities of energy by incident particles or by any heterogeneous nucleation sites such as gas pockets or impurities disturbs the energy balance in the liquid and locally vaporizes the liquid. Because the vapor pressure is higher than the surrounding liquid pressure, the

newly formed bubble tends to expand, but the expansion force is counterbalanced by the surface tension force at the gas–liquid boundary.¹² Other factors influencing the bubble growth are the viscosity force that slows down the bubble expansion and the force transmitted to the bubble growth from the bubble/wall interaction. If the radius of the generated bubble is greater than a certain critical value R_c , the force balance is dominated by the vapor pressure and the bubble continues to grow (otherwise the bubble is reabsorbed into the liquid). As a fraction of the chamber volume vaporizes through the nucleation process, the liquid pressure inside the active medium increases until a balance is reached for a bubble radius of macroscopic size. After a short interval of time (usually a few tens of milliseconds), the bubbles fill the chamber and the boiling spreads to the whole liquid volume.¹² The chamber has to be repressurized to clean the gas pockets resulting from boiling and then decompressed again to take a new set of data. For the particular case of a gel detector, the active medium is represented by tiny pressurized liquid drops suspended in a transparent gel. Due to the higher pressure, these drops are in a superheated state and each of them behaves as a miniature bubble chamber.¹² The mechanism of bubble formation works in the same way as a liquid bubble chamber.⁸

The minimum energy E_b necessary for the formation of a bubble of critical radius R_c is described by^{13,14}

$$E_b = W_b + H + E_{\text{wall}} + E_{\text{visc}}, \quad (1)$$

where W_b is the minimum reversible work required for bubble formation, H is the vaporization energy, E_{wall} is the kinetic energy transmitted to the liquid during the growth process, and E_{visc} is the energy lost during the bubble growth by viscous forces.¹⁵ E_{wall} and E_{visc} can be neglected in this work.^{16,17} During the nucleation process, the bubble forms so rapidly that there is no time for energy exchange to take place between the bubble and the surrounding liquid.¹⁴ Once the bubble is initiated, the energy required to maintain it is given by the minimal reversible work W_b expressed as

$$W_b = 4\pi r^2 \gamma(T) - \frac{4}{3}\pi r^3 (p_v - p_0), \quad (2)$$

where $\gamma(T)$ is the liquid–vapor interfacial tension (temperature dependent), p_v is the vapor pressure of the superheated liquid, and p_0 is the ambient liquid pressure. The difference $p_v - p_0$ is called the degree of superheat of a given liquid. W_b is minimized for a critical radius

$$R_c = \frac{2\gamma(T)}{p_v - p_0}. \quad (3)$$

When a bubble reaches its critical radius, its vapor pressure is greater than its surface tension force. It becomes thermodynamically unstable and grows quickly. Once the liquid has vaporized locally, the minimum amount of energy W_b needed to form a vapor bubble of critical size R_c , as given by Gibbs (1875)¹³ from reversible thermodynamics, is

$$W_b = \frac{16\pi\gamma^3(T)}{3(p_v - p_0)^2}. \quad (4)$$

The vaporization energy can be expressed as^{14,18}

$$H = \frac{4}{3}\pi R_c^3 \rho_v H_v \quad (5)$$

with ρ the vapor density and H_v the latent heat of vaporization. Replacing Eqs. (4) and (5) in Eq. (1) and neglecting the kinetic and viscous energies, the minimum energy necessary to produce a bubble can be expressed as

$$E_b = \frac{16\pi\gamma^3(T)}{3(p_v - p_0)^2} + \frac{4}{3}\pi R_c^3 \rho_v H_v. \quad (6)$$

Equation (6) can be rewritten as

$$E_b = W_b \left(1 + \frac{\rho_v H_v}{p_v - p_0} \right). \quad (7)$$

Equation (7) accounts for the conversion efficiency (η) of heat to work, described by the relation

$$\eta = \frac{W_b}{E_b}. \quad (8)$$

For typical superheated liquids (Freon 12, Freon 115, Freon 134a), the value of η ranges from 2% to 6%.¹⁹ The energy necessary to create a bubble, E_b , is supplied through the energy deposition per unit length dE/dx by the electrons ejected by the recoil nuclei.¹⁸ The bubble nucleation requirements for a superheated medium are satisfied if the incident particle deposits enough energy to create a bubble within a specified length L , given by

$$L = k_b \cdot R_c, \quad (9)$$

where k_b is a constant that may vary between 2 and 13, in most cases being approximated as 2 (Refs. 16 and 19). The nucleation requirement is satisfied if [cf. Eq. (8) and (9)]

$$\frac{dE}{dx} \geq \frac{E_b}{k_b \cdot R_c} = \frac{W_b}{\eta \cdot k_b \cdot R_c}. \quad (10)$$

The condition necessary to create a bubble can be expressed as a minimum energy density ρ_E deposited over a sphere of radius R_c :

$$\rho_E \geq \frac{3E_b}{4\pi R_c^3}. \quad (11)$$

Replacing the values for the Freon 115 bubble chamber at 50°C (Ref. 20) (the operating temperature of the OMEGA bubble detector^{9,10}) in Eq. (6), the critical radius is $R_c = 7.5 \times 10^{-9}$ m and the minimum energy necessary to generate a bubble is $E_b = 107$ eV.

Bubble chambers operate at a quasi-constant temperature and therefore behave as isothermal systems. W_b can be obtained from the difference between the liquid pressure in the superheated state and the pressure of the foam limit.^{21,22} A bubble chamber is sensitive to particle detection only in its superheated state. The conditions necessary to reach this state depend on the thermodynamic-phase diagram of the liquid used as the active medium. Figure 121.39 shows the phase diagram for Freon 115.²² The medium is in the liquid state above the vapor pressure line, gaseous below the foam limit line, and in a metastable coexistence state in the middle. During the bubble chamber operation the temperature is held constant while the pressure decreases quickly from a point on the upper curve (start/stable) to a value close to the lower curve (working unstable), where it is ready to record any interactions with the incident particles. The detector sensitivity and the bubble growth speed depend on temperature. Measurements made at CERN in the 1980s found that the bubble density for Freon 115 reaches maximum at 48°C (Ref. 22). For the bubble detector used on OMEGA,^{9,10} the position of the piston during the decompression and the quantity of the Freon inside the chamber suggested that an operating temperature of 50°C was optimal.

The lines of constant bubble density come closer to the foam limit at higher temperatures. For a different active medium, the nominal values described in Fig. 121.39 may vary widely, but all liquid bubble chambers operate with the same principle. The foam limit is reached at the pressure $p^*(T)$, which is estimated, according to Bugg,²³ to be

$$p^*(T) = P_v - K \sqrt{\frac{k_L T}{\gamma^3}}, \quad (12)$$

where p_v and γ are the vapor pressure and surface tension, respectively, at the temperature T , k_L is the thermal conductivity of the liquid, and K is a numerical proportionality constant determined experimentally (in most cases close to 1).

The bubble growth rate can be estimated from the formula deduced by Plesset and Zwick:²⁴

$$r = A \sqrt{t} \quad (13)$$

with

$$A = 2 \sqrt{\frac{3}{\pi}} \sqrt{k_L \rho c_l (T_\infty - T_b)} / H_v \rho', \quad (14)$$

where k_L is the thermal conductivity of the liquid, ρ is its density, c_l is the specific heat, H_v is the heat of vaporization, ρ' is the density of the gas, T_∞ is the temperature of the liquid, and T_b is the temperature of the bubble (at the same pressure). The difference, $T_\infty - T_b$, decreases as the temperature increases. Equation (14) shows that the bubble growth rate decreases with increasing temperature. The effect of bubble movement caused by buoyancy forces and the effect of the spatial variation of the pressure during the bubble chamber cycle have been neglected during the bubble growth process.²² Table 121.X, adapted from Ref. 22, shows the change of A as a function of temperature.

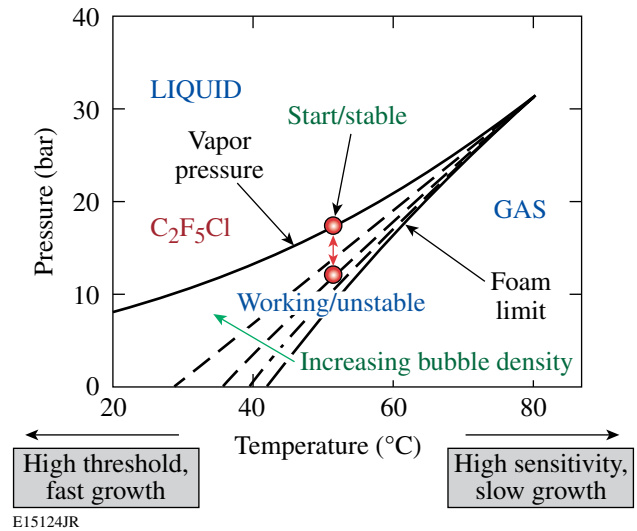


Figure 121.39

Bubble production as a function of pressure and temperature in a Freon 115 bubble chamber. The working region is the area between the vapor pressure line and the foam limit line. The dashed lines represent lines of constant bubble density (adapted from Ref. 20).

Table 121.X: Heat content and bubble growth rate for Freon 115 and hydrogen as functions of temperature (from Ref. 19).

Liquid	Temperature	$A(\text{cm}/\sqrt{\text{s}})$	Heat content (cal)
$\text{C}_2\text{F}_5\text{Cl}$	48°C	0.35	1.2×10^{-5}
	55°C	0.10	5.0×10^{-7}
	60°C	0.046	5.9×10^{-8}
	65°C	0.023	8.6×10^{-9}
H_2	29 K	0.095	9.3×10^{-8}

Equations (13) and (14) show that the development of an average bubble radius depends on both the temperature and time after initiation as shown in Fig. 121.40. From the temperature fluctuations inside the chamber, an active medium (Freon 115) variation range for parameter A was estimated. A temperature difference of 0.2°C between two Freon regions inside the chamber induces a 2% difference in the bubble-growth speed.

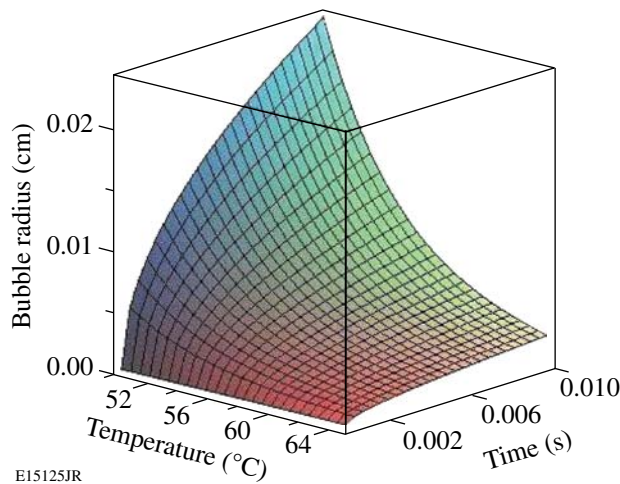


Figure 121.40
The average bubble radius as a function of temperature and time for Freon 115.

2. The Thermodynamic Mechanism of Bubble Formation in Freon 115

The mechanism of bubble generation inside a bubble chamber depends on the production of highly localized regions where heat is released (“temperature spikes”) within the active medium. These areas quickly expand into bubbles larger than the critical radius R_c [described by Eq. (3)] and grow through the evaporation of the superheated liquid.¹⁸

An incident neutron will interact with the sensitive medium inside a bubble chamber as follows:¹⁸

1. A percentage of the neutrons that reach the liquid scatter elastically off the nuclei of the constituent molecules. During this interaction, the neutrons eject charged nuclei from these molecules (C, F, Cl for Freon 115).
2. The ejected nuclei interact with molecules of the active medium, freeing nuclei or electrons from the medium atoms or moving the bound electrons to excited states.
3. The ejected electrons lose their energy inside the medium over a distance proportional to their initial velocity, ejecting more electrons. The recombination of the free electrons and ions/nuclei or the return of the electrons from their excited states to stable energy levels release energy that behaves as a “temperature spike.” When these processes occur in a quasi-spherical zone of volume $\sim R_c^3$, a bubble is generated.

The number of bubbles produced inside a neutron detector depends on the neutron path inside the active medium (directly related to the bubble chamber’s size), the neutron yield, the geometry of the experiment (the distance from the neutron source to the detector influences the solid angle), and the efficiency of the bubble creation mechanism by the incident neutrons. From previous experimental measurements, the total neutron-scattering cross sections are known to be $S_C = 1.30$ barn for carbon, $S_{Cl} = 2.0$ barn for chlorine, and $S_F = 0.053$ barn for fluorine.²⁵ The total cross section is $S_t = 4.865$ barn for a Freon molecule (8 atoms) that has a mass of $M = 154.5$ atomic units. The total cross section of the medium can be estimated from the detector volume. By taking the ratio between the total cross section and the detector cross section, the fraction of the incident neutrons interacting with the medium is determined.

To create a bubble, the energy released by the neutron has to reach the value E_b described in Eq. (5). Elastic collisions are described by a set of equations describing the conservation of momentum and energy:

$$\begin{aligned}
 m_n v_n + m_i v_i &= m_n v'_n + m_i v'_i \\
 \frac{m_n v_n^2}{2} + \frac{m_i v_i^2}{2} &= \frac{m_n v'^2_n}{2} + \frac{m_i v'^2_i}{2},
 \end{aligned}
 \tag{15}$$

where m and v represent the mass and velocity, with the indices “n” and “i” standing for the neutron and the recoil ion, respectively, and the prime annotation indicating the particles after interaction. The Freon molecules are at rest compared with the

high velocity of the incident neutrons, $v_i = 0$, and the maximum velocity of the recoil ion is (for a 180° scattering angle)

$$v_i' = \frac{2m_n v_n}{m_n + m_i}. \quad (16)$$

A fraction of the incident neutrons will interact with the Freon and eject nuclei from its molecules. Based on the 14.1-MeV initial energy of the neutrons and the dynamics of the elastic scattering, the final kinetic energy of the ejected nuclei can range from 0 MeV to ~ 4 MeV for the carbon ions (the lightest components from the Freon molecule). It takes 2 keV to 5 keV to completely ionize an atom of C, Cl, or F (only 11 to 17 eV to singly ionize it, depending on the atom species), so, for a first approximation, the ionization energies can be neglected.

The stopping power for heavy-charged particles in the classical regime (with $E \ll m_0 c^2$) is described by the Bethe–Bloch equation^{26,27}

$$S_i = \frac{Zz^2 e^4 N_A m_i}{8\pi \epsilon_0^2 m_e E_{\text{kin}} M_A} \cdot \rho \cdot \ln \left(\frac{3m_e E_{\text{kin}}}{2\bar{T} m_i} \right), \quad (17)$$

where the stopping power is expressed in MeV/cm, Z is the atomic number of target atoms, z is the atomic number of the charged particle, N_A is Avogadro's constant (mol^{-1}), m_e is the rest mass of the electron (kg), ϵ_0 is the electric permittivity of free space ($C \cdot V^{-1} \cdot m^{-1}$), E_{kin} is the kinetic energy of the particle (J), M_A is the molar mass of the target (g/mol), \bar{T} is the mean ionization energy (J), ρ is the medium density (kg/m^3), and e is the electron charge.

Using the SRIM software designed by James Ziegler (<http://www.srim.org>, based on the Bethe–Bloch equation and experimental data from many sources), the scattered ion range was found to be between $\sim 0 \mu\text{m}$ and $9 \mu\text{m}$, depending on the atom type and recoil ion energy. Each bubble produced inside the active medium expands from a very small volume associated with the transfer of the threshold energy E_b to either an electron or a nucleus from the incident particle as a result of Rutherford scattering.

The case where a recoil ion ejects further nuclei from the active medium molecules deserves a quick analysis. The cross section σ_p for ejecting a nucleus varies with $1/E_c$ in the Rutherford range, where E_c is the kinetic energy of the incident particle.¹⁸ For a given energy $E \geq E_b$, a simple calculation of

the ratio of the cross sections necessary to eject a nucleus and an electron is given by¹⁸

$$\frac{\sigma_p}{\sigma_e} = \frac{n_m m_e}{Z_e M_n}, \quad (18)$$

where n_m is the number of nuclei per molecule, m_e is the electron mass, Z_e is the number of electrons per molecule (the sum of the component atomic numbers), and M_n is the mass of the nucleus. The average mass for the nucleus of a Freon 115 molecule is $M_n = 19.3$ and $Z_e = 74$. Replacing all the values in Eq. (6), the obtained interaction cross-section ratio is $\sigma_p/\sigma_e \cong 3 \times 10^{-6}$. The fraction of the ejected nuclei that produce bubbles is only 3×10^{-6} of the number of electrons creating bubbles, so it can be neglected. Essentially all the bubbles generated by incident neutrons originate from free electrons ejected by recoil ions.

To measure the energy transferred to electrons by an ejected nucleus, one has to know the stopping power for a particle moving inside a medium. This is defined as the differential energy loss dE along the path element dx :²⁷

$$S = -\frac{dE}{dx}. \quad (19)$$

Using data obtained from simulations with the SRIM software, the stopping power's dependence on the ion energy has been plotted in Fig. 121.41.

To satisfy the minimum nucleation conditions, Eq. (9) must be true for the ion energy loss inside the superheated medium. If minimum energy loss/distance to create a bubble is written as L_b and the energy loss/distance for the recoil ion as L_i , the nucleation condition is satisfied for $L_i \geq L_b$. When this is satisfied, it does not mean that a bubble is created since bubble formation requires the electrons resulting from the recoil ion collision with the medium molecule electronic layers to have both the minimum nucleation energy and the minimum range, while the nucleation centers are too close to each other and will fuse quickly into a single visible bubble. In most cases, however, $L_i \leq L_b$ and the nucleation occurs with a probability depending on the energy loss per volume since Eq. (10) also needs to be satisfied. For the case of ions with low energies (valid for the case of 14-MeV neutron detection inside Freon 115), the number of bubbles generated by a recoil ion moving over a distance equal to the critical diameter can be expressed as

$$N_i = \alpha \cdot \left(\frac{L_i}{L_b} \right)^3, \quad (20)$$

where the third power is due to the volumes' ratio and α is a proportionality coefficient representing the energy conversion efficiency from the free electrons to the medium. Based on previous literature,^{12,14} this conversion efficiency is close to 1 and the bubbles' density depends on the energy loss of the ejected ions inside the superheated medium.

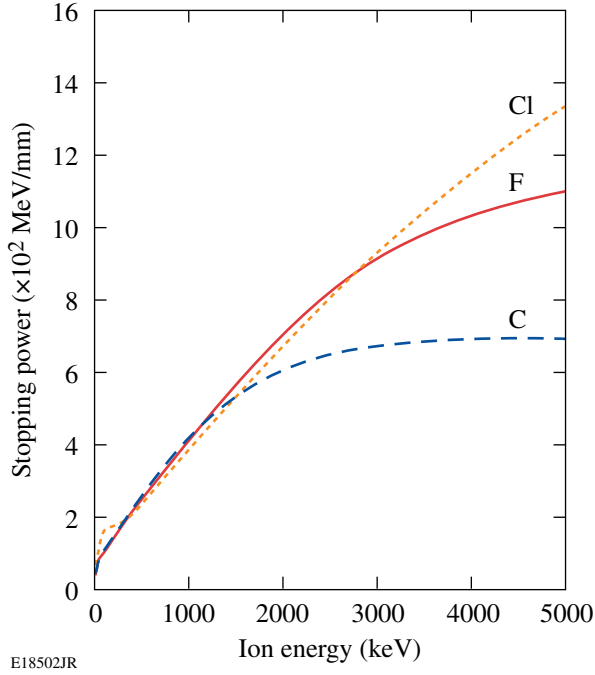


Figure 121.41
The total stopping power derived from SRIM simulations for ions of carbon, fluorine, and chlorine inside Freon 115.

3. The Stopping Power for Electrons Inside Freon 115

For electrons, the stopping power is calculated using the adapted Bethe–Bloch formula and expressed in MeV/mm (Ref. 27):

$$S_e = \frac{Ze^4 N_A}{8\pi\epsilon_0^2 m_e v^2 M_A} \cdot \rho \cdot \ln \left[\frac{m_e v^2 E_{kin}}{\bar{I}^2 (1 - \beta^2)} \right] + f(\beta), \quad (21)$$

where Z is the atomic number of the target atom, N_A is the Avogadro's constant (mol^{-1}), m_e is the rest mass of the electron (kg), ϵ_0 is the electric permittivity of free space ($C \cdot V^{-1} \cdot m^{-1}$), E_{kin} is the kinetic energy of the electron (J), M_A is the molar mass of the target (g/mol), \bar{I} is the mean ionization

energy (J), v is the electron velocity (m/s), ρ is the medium density (kg/m^3), e is the electron charge, $\beta = v/c$ with c the speed of light, and $f(\beta)$ is a relativistic correction function.

Using the ESTAR program designed by the National Institute of Standards and Technology (NIST) (<http://physics.nist.gov>), based on Eq. (21) and experimental measurements, the electron range r_e is multiplied by the density to give an areal density and is calculated by ESTAR in a similar way and displayed in Fig. 121.42(a). This value can be misleading since the electrons interact with the medium and do not move on straight trajectories. The actual range is about 30% less than that calculated by ESTAR. The electron stopping power inside Freon 115, normalized to the medium density, was calculated as shown in Fig. 121.42(b).

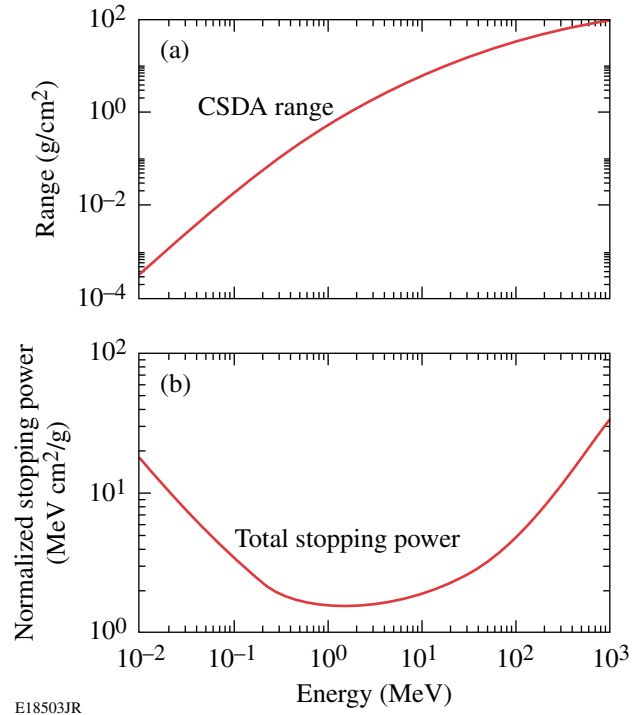


Figure 121.42
(a) The electron range multiplied by density inside Freon 115 and (b) the total stopping power for electrons inside Freon 115, normalized to the medium density.

The expression for the cross section (in cm^2) for an interaction between a nucleus and an electron (derived from the Rutherford formula) is (adapted from Ref. 18)

$$\sigma_{e,m} = 18.74 \times 10^{21} \frac{Z_e R_h}{E_b \beta^2} (\text{cm}^2), \quad (22)$$

where Z_e is the number of electrons/molecule, R_h is the Rydberg energy (13.6 eV), E_b is the threshold energy to create a bubble, and β is the ratio between the velocity of the incident particle (recoil ion) v and the speed of light c . As expressed by Eq. (22), $\sigma_{e,m}$ decreases with the recoil ion velocity.

Cross section, molecule concentration, and average molecular radius can be calculated from the medium density and molar mass. The fraction of electrons with energies high enough to cross a distance equal to the critical bubble diameter can be then expressed as

$$\alpha = \frac{\sigma_{e,m}}{\sigma_{\text{mol}}} \cdot \frac{r_d}{2R_c}, \quad (23)$$

where σ_{mol} is the molecule cross section, r_d is the ion recoil distance, and R_c is the bubble's critical radius. Combining Eqs. (20) and (23), the number of bubbles generated by a recoil ion becomes

$$N_i = \frac{\sigma_{e,m}}{\sigma_{\text{mol}}} \cdot \frac{r_d}{2R_c} \cdot \left(\frac{L_i}{\beta L_b} \right)^3. \quad (24)$$

Extending the calculations for a neutron detector, the sensitivity of a bubble chamber to neutrons can be expressed as

$$\begin{aligned} \frac{N_{\text{bubbles}}}{n_{\text{source}}} &= F_n \cdot N_i \cdot d\Omega \\ &= F_n \cdot \frac{\sigma_{e,m}}{\sigma_{\text{mol}}} \cdot \frac{r_d}{2R_c} \cdot \left(\frac{L_i}{\beta L_b} \right)^3 d\Omega, \end{aligned} \quad (25)$$

where F_n is the fraction of the incident neutrons interacting with the active medium and $d\Omega$ is the detector's solid angle. If this mechanism of bubble formation is valid, the value of $N_{\text{bubbles}}/N_{\text{source}}$ can range between 10^{-5} for a gel detector and 10^{-3} for a liquid detector. Unfortunately, as shown below, Eqs. (24) and (25) work only for a gel detector and for some liquid detectors. Freon 115 has a very small critical radius so the energy density required to generate a bubble cannot be reached based on the stopping power of the electrons ejected by the recoil ions.

The Mechanism of Bubble Formation for a Small Critical Radius

For nucleation to occur, the operating conditions must be in the thermodynamic limit, with critical radii in the range of

20 nm or larger and bubble threshold energies in the range of 1 keV or higher. An electron ejected by an incident particle ejects other electrons with relatively low energies. The incoming electron interacts with the orbital electrons in the medium, producing multiple new electrons (and ions) with lesser energy; each of these then interacts in the same way—a process that continues until many low-energy particles are produced. These are then stopped in the medium and absorbed. This process is known as a particle shower.

For very small critical radii, the volume of the critical bubble encloses only a few tens of molecules and the thermodynamic equations of bubble formation do not describe the nucleation process accurately. For example, for the case of Freon 115 at 50°C, the critical radius for bubble formation is 7 nm. Although the threshold energy for bubble generation decreases to ~100 eV for this volume, an electron with such a low energy has a range that is much less than the critical diameter. Its energy is transmitted to the medium over a range much smaller than the critical radius, and the bubble will collapse before it can nucleate. Even though an electron with a higher energy (500 eV) has a recoil range comparable to a critical bubble diameter, most of its energy will be lost while ejecting a small number of low-energy electrons that are immediately absorbed.

The software package CASINO (Monte Carlo simulation of electrons in solids, available for download at <http://www.srim.org/SREM.htm>), designed by Raynald Gauvin (Université de Sherbrooke, Québec, Canada), was used to calculate the electron ranges in Freon 115 at low energies. The average range of the electrons is ~14 nm (i.e., twice the critical radius). Electrons with energies higher than 500 eV will dissipate their energies over radii larger than the critical radius, while electrons with energies lower than 500 eV will not have enough energy to generate a shower of secondary particles that could fill the volume of a critical-radius bubble. For this reason, any generated micro bubble will quickly collapse before it can be observed. The mechanism of bubble formation based on the ejected electrons' stopping power does not work for media with a small critical radius, such as Freon 115.

For high-energy recoil ions, the dominant process that generates bubbles consists in the excitation of active medium molecules' electronic levels. This happens for energy values in excess of¹⁸

$$E_{\text{ex}} = \frac{M_i Z_i E_e}{m_e}, \quad (26)$$

where M_i is the mass of the incident particle (recoil ion), Z_i is the particle charge, and E_e is the first electronic excitation energy (13.6 eV). The excitation of the electronic levels releases energy quite uniformly inside a volume of a sphere of critical radius, and the distance between successive excited molecules will be less than the molecular mean free path. The nucleation process can be affected by the thermal motion since the growing bubble can break apart and collapse because of the random movement of molecules over the nucleation region. As shown in Eq. (22), the probability that a particle will eject a high-energy electron decreases with its energy. For very high energy particles, the probability of ejecting an electron drops to practically zero while the excitation of the electronic levels becomes the main mechanism for energy loss.¹⁸ Consequently, even for small critical radii, nucleation is possible for energies of the incident particles within the MeV range.

The probability of bubble generation for a recoil nucleus can be estimated from the ratio of the cross section for the first electronic-level excitation energy to the cross section of a critical radius bubble (as in this case where the energy is transmitted through the excitation of the electronic levels) and the nuclear recoil distance. The cross section for the first electronic-level excitation energy is difficult to estimate. It can be approximated using Eq. (26) to calculate the cross section to generate energies higher than the excitation level and subtracting from it the cross section for energies close to the E_b value (the energy necessary to create a bubble), which will generate more-energetic electrons that produce ionization in the medium and induce nucleation. Based on this approximation, the following equation provides a general estimate for the number of bubbles created by a recoil ion rather than an exact value:

$$N_{\text{ieex}} = \eta \left(\frac{\sigma_{\text{ex}} - \sigma_{\text{eject}}}{\pi R_c^2} \cdot n_{i,n} \right)^{\frac{E_b}{E_e}} \cdot \frac{r_d}{2R_c}, \quad (27)$$

where η is a correction coefficient that depends on the thermal influence for the bubble formation and must be determined experimentally, σ_{ex} is the cross section for a recoil ion to transmit the excitation energy E_e to an electron, σ_{eject} is the cross section for a recoil ion to eject an electron, R_c is the critical radius, E_e is the first electronic excitation energy, $n_{i,n}$ is the average number of interactions for which an electron of energy E_e is generated, E_b is the energy necessary to create a bubble, and r_d is the recoil ion range.

Adapting the calculations to a neutron detector, the bubble chamber's sensitivity to neutrons can be expressed as

$$\begin{aligned} \frac{N_{\text{bubbles}}}{n_{\text{source}}} &= F_n F_{\text{ex}} N_{\text{ieex}} d\Omega \\ &= F_n F_{\text{ex}} \eta \left(\frac{\sigma_{\text{ex}} - \sigma_{\text{eject}}}{\sigma R_c} \cdot n_{i,n} \right)^{\frac{E_b}{E_e}} \cdot \frac{r_d}{2R_c} d\Omega, \end{aligned} \quad (28)$$

where F_n is the fraction of the incident neutrons interacting with the active medium, F_{ex} is the fraction of carbon nuclei that can generate bubbles by exciting the electronic systems of the active medium, η is a thermal coefficient that must be determined experimentally, and $d\Omega$ is the detector's solid angle. With the exception of η , all of the factors can be estimated from theoretical calculations.

Calculation of the Thermal Coefficient η Based on Data from a Freon 115 Bubble Chamber Used at CERN

Bubble tracks were recorded by a Freon 115 detector designed and built at CERN in 1981.²⁸ The nucleations were generated by incident 360-GeV/c protons inside an externally induced magnetic field. The recorded bubble density along the charged-particle tracks was in the range of 160 bubbles/cm at 50°C, decreasing with temperature. Based on the SRIM simulations, the stopping power for charged particles decreases with increasing energy. For protons, it reaches a minimum of 0.2 MeV/mm at 2.75 GeV and increases slowly, reaching 0.3 MeV/mm at energies over 100 GeV/c (Ref. 29). For the operating conditions of the CERN bubble chamber, the pressure difference was in the range of 10 bar, with a critical bubble radius $R_c = 4.3$ nm at 50°C and $R_c = 2.6$ nm at 60°C. At high energies, the only possible interactions are those that excite the electronic levels (the interaction time is very short), and the interaction efficiency is close to 1. Equation (21) for the number of bubbles generated by a recoil ion can be rewritten as

$$N_i = \frac{r_d}{2R_c} \cdot \left(\frac{L_i}{L_b} \right)^3, \quad (29)$$

where r_d is the ion recoil distance, R_c is the critical bubble radius, L_b is the minimum energy loss/distance to create a bubble, and L_i is the energy loss/distance for the recoil ion. Using Eq. (29) the linear bubble density should be 429 bubbles/cm at 50°C and 155 bubbles/cm at 60°C.

The qualitative explanation is that the very small bubble radius and the thermal motion inside the liquid may disrupt and prevent the bubbles from nucleating. Using the data provided by Okada *et al.*,²⁰ describing the dependence of the Freon surface tension for Freon 115 as a function of temperature and

knowing the pressure drop during the chamber decompression, the critical radius for the bubble formation can be calculated using Eq. (3). Correlating the bubble's critical radius with the observed number of bubbles, a linear dependence of η with critical bubble radius was determined, as shown in Fig. 121.43. The η factor explains the discrepancies between the calculated and experimentally measured values.

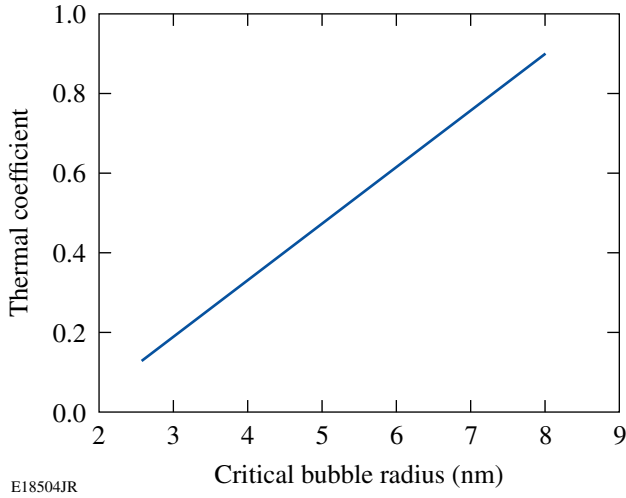


Figure 121.43
The thermal coefficient as a function of the critical bubble radius inside Freon 115.

For the experimental conditions encountered on OMEGA, the critical radius was in the range of 7 nm, so the thermal coefficient has a value of $\eta = 0.75$. In conclusion, the thermal motion affects bubble formation even for the mechanism of bubble formation involving the excitation of the electronic levels, and the bubble density decreases linearly with the increasing temperature.

Numerical Estimate for the Number of Nucleations Generated by 14.1-MeV Incident Neutrons Inside Freon 115

For Freon 115, the value of E_{ex} is 1.8 MeV for carbon, 4.2 MeV for fluorine, and 15.9 MeV for chlorine. Based on the recoil ion energies achieved from the elastic interactions with the incident 14.1-MeV neutrons, the maximum recoil energy is 4 MeV for carbon, 2.7 MeV for fluorine, and 1.5 MeV for chlorine. Equation (26) indicates that only the carbon recoil nuclei (ions) may have enough energy to generate nucleation inside Freon 115 by exciting the electronic system of the active medium molecules. The carbon recoil nuclei have an energy of 1.8 MeV or greater at a scattering angle of 50° .

Using the differential cross section for 14.1-MeV neutron elastic scattering on carbon shown in Fig. 121.44,³⁰ the fraction of carbon nuclei that can generate bubbles, F_{ex} , through the mechanism of exciting the electronic systems of the active medium can be estimated to be about 10% of the nuclei with which the incident 14.1-MeV neutrons interact.

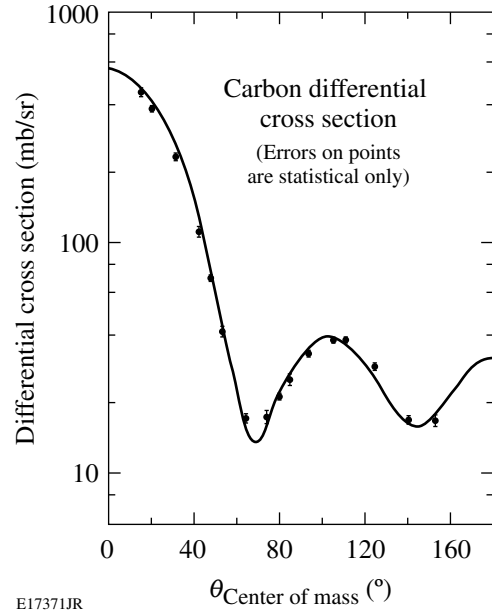


Figure 121.44
The differential cross section for 14-MeV neutron elastic scattering on carbon. About 98% of the recoil ions have energies greater than the threshold energy E_b necessary to generate a bubble (from Ref. 27).

The neutron-carbon cross section F_C represents 53% of the total cross section of Freon 115. Multiplying this value by F_n , one obtains the fraction of the incident neutrons interacting with the active medium that can theoretically generate bubbles inside Freon 115.

Based on Freon 115's density (1.15 g/cm^3) and molecular mass ($M = 154.5$ atomic units), the concentration of Freon molecules per cm^3 is $N_f = 4.99 \times 10^{21}$. This gives an average distance between molecules of $d_{\text{mol}} = 5.8 \times 10^{-8} \text{ cm}$ and a cross section for the volume occupied by a molecule of $\sigma_{\text{mol}} = 2.689 \times 10^{-15} \text{ cm}^2$ from Eq. (29).

The value of d_{mol} is used to estimate the factor

$$\left(\frac{\sigma_{\text{ex}} - \sigma_{\text{eject}}}{\sigma R_c} \cdot n_{i,n} \right)^{\frac{E_b}{E_e}} \approx 6.4 \times 10^{-8}.$$

The average recoil distance for carbon at energies between 1.8 MeV and 4 MeV is around $7 \mu\text{m}$ and $r_d/2R_c \approx 500$. With the thermal coefficient $\eta = 0.75$, the number of bubbles generated by a neutron that interacts with the medium and shape equivalent to that of the prototype detector used for neutron detection on OMEGA is

$$\frac{N_{\text{bubbles}}}{n_{\text{interact}}} = F_C F_{\text{ex}} N_{\text{icx}} = 5.8 \times 10^{-6}. \quad (30)$$

The detector is a 3.5-cm-diam, 10-cm-long cylinder. As specified in the previous section, the total cross section for the 14-MeV neutrons scattering on Freon is $S_t = 4.8$ barn (the Freon molecular mass is $M_{\text{Fr}} = 154.5$ atm). By knowing the active medium density, one can calculate the total cross section of the liquid. Freon has a density of 1.15 g/cm^3 at 50°C , so the corresponding mass for the volume is $m_f = 110$ g. As already shown, the fraction of the neutrons interacting with the Freon inside the detector is ≈ 0.22 and the solid angle of the detector is $d\Omega = 1.2 \times 10^{-6}$.

Substituting these values in Eq. (28), one obtains the estimated number of bubbles per source neutron $N_{\text{bubbles}}/n_{\text{source}} = 1.5 \times 10^{-12}$ or for the number of bubbles expected to be observed inside the detector, $N_{\text{det}} \approx 15$ for a neutron yield of 10^{13} . This low value for the number of bubbles created inside Freon 115 indicates that the Freon bubble chamber is not sensitive enough for neutron imaging for the yields achieved on OMEGA but may be appropriate for the higher yields produced at the NIF, where the neutron yield is expected to approach 10^{19} . These calculations were tested against experimental measurements with a Freon 115 bubble chamber. The experimentally observed values of $N_{\text{meas}} \approx 11$ to 14 bubbles agreed with these theoretically calculated values.¹⁰ If it were possible to use a liquid bubble chamber with Freon 115 at room temperature, the critical radius described by Eq. (4) would increase to ~ 20 nm and the ejected electrons would become dominant for bubble formation, as described previously. The number of observed bubbles should reach much higher values when calculated by Eq. (30) ($\sim 10^6$ bubbles). Unfortunately, for temperatures lower than 48°C , foaming occurs inside Freon 115 before any useful data can be recorded.¹¹

Numerical Estimate for the Number of Nucleations Generated by 14.1-MeV Incident Neutrons Inside a Gel Detector

Freon gel detectors were used to record 14.1-MeV neutrons on OMEGA in 2001.⁸ Disk-shaped gel bubble detectors,

8.5 cm in diameter and 1 cm thick, were installed behind the penumbral neutron aperture and close to the outside edge of the OMEGA target chamber. The detectors consisted of 10^5 droplets, approximately $3 \mu\text{m}$ in diameter, of a superheated liquid (Freon) suspended in an elastic polymer matrix support gel.⁸ The gel material has no effect on bubble generation.³¹ The neutron-imaging system's aperture was biconical, with a 0.75-mm inner diameter. The target-to-detector distance was 362 cm and the target-to-aperture distance was 8 cm, with a system magnification $M \approx 45$ (Ref. 8). The neutron yield was 6×10^{13} (Ref. 8).

Depending on the Freon type used, the calculated critical radius R_c at 22°C to 23°C can range from 20 nm to 40 nm with the energy necessary to create a bubble in the range of 1 keV to 5 keV. At these energies, the mean free path of the electrons ejected by the recoil nuclei inside the gas is about 20 nm to 40 nm, and the distance between two consecutive ejected electrons is shorter than the molecular mean free path of 1 nm to 3 nm, filling the critical bubble volume continuously with heat spikes resulting from the subsequent recombination of ions and electrons. As a result, the heat is released in a volume comparable to the volume of the critical radius for bubble formation R_c , the mechanism of bubble creation is valid, and Eq. (24) can be used.

The stopping power calculated for the recoil ions generated by incident 14.1-MeV neutrons inside Freon using the SRIM software is in the range of 400 MeV/mm, while the energy necessary to create a bubble along the particle trajectory is significantly lower, at 50 to 90 MeV/mm. On the molecular scale, most of the recoil ions (nuclei) will generate many electrons that can fill a critical bubble volume with enough energy to induce nucleation along its path. Since the ions have recoil ranges up to $9 \mu\text{m}$ (with an average value of $2 \mu\text{m}$), they will create a continuous track of bubbles that will grow rapidly and fuse into larger bubbles. These bubbles will fill the $3\text{-}\mu\text{m}$ superheated droplets and can be recorded.

The neutron-Freon interaction cross section is in the range of 4.2 barn for both Freon 12 and Freon 22. Using a similar calculation as for Freon 115, the neutron-detection efficiency per source neutron is estimated to be 0.021 for the 1-cm-thick gel detector, assuming it is filled entirely with Freon. Since only 0.1% of the detector's volume is actually filled with Freon, the detection efficiency is

$$\frac{N_{\text{bubbles}}}{n_{\text{source}}} = 2.1 \times 10^{-5} d\Omega. \quad (31)$$

Based on the geometry of the imaging system, the radius of the central maximum at the detector is $r \approx 3$ cm. The number of neutrons reaching the detector can be calculated using the formula

$$N_i = \frac{y \cdot r^2}{4 \cdot R^2}, \quad (32)$$

where y is the neutron yield, r is the radius of the detector, and R is the distance between the neutron source and detector. Inserting the numerical values into Eq. (32), the number of the neutrons entering the Freon medium is $N_i = 2.6 \times 10^8$. The solid angle of the detector is $d\Omega = 4.3 \times 10^{-6}$. Multiplying N_i by the neutron-detection efficiency per source neutron, the estimated number of bubbles inside the central maximum area is

$$N_{\text{bubbles}} = N_i \cdot \frac{N_{\text{bubbles}}}{n_{\text{source}}} = 5.4 \times 10^3. \quad (33)$$

The testing of gel detectors on OMEGA in 2001 measured 5.3×10^3 bubbles.⁸

Conclusions

Based on the classical mechanism of bubble formation, the interaction between an incident neutron and the sensitive medium inside a bubble takes place in three steps: first, the medium nuclei are elastically scattered; second, the scattered nuclei generate free electrons; and, third, the free electrons recombine with the ions over a quasi-spherical volume to generate bubbles.

The efficiency of nucleation depends on both the size of the critical radius and the medium temperature. For some particular cases, as in the use of Freon 115 on OMEGA, the critical radius is shown to be too small for bubble generation through the mechanism of free electron-ion recombination. Some bubbles are generated, however, through the excitation of electronic levels by charged incident particles at relatively high energies (MeV range).

For a bubble chamber used on OMEGA, the estimated number of bubbles per source neutron is calculated to be $N_{\text{bubbles}}/n_{\text{source}} = 1.5 \times 10^{-12}$, or for the number of bubbles observed inside the detector (after subtracting the turbulence area), the expected value is $N_{\text{det}} \approx 15$. These values agree with the experimentally recorded $N_{\text{meas}} \approx 11$ to 14 bubbles on OMEGA.¹⁰ The expected number of bubbles for the experi-

mental conditions encountered on OMEGA is insufficient for neutron imaging, but the higher yields from the NIF will be able to create a high-enough bubble density for a useful diagnostic tool, provided a similar but improved system is used.

Because of the lower temperature and larger (20-nm) critical radius, a simplified model of bubble formation that does not take into account the size of the critical radius gives accurate results for gel detectors. The numerical predictions of this model agree with the results obtained on OMEGA in 2001.⁸

ACKNOWLEDGMENT

This work was supported by the U.S. Department of Energy Office of Inertial Confinement Fusion under Cooperative Agreement No. DE-FC52-08NA28302, the University of Rochester, and the New York State Energy Research and Development Authority. The support of DOE does not constitute an endorsement by DOE of the views expressed in this article.

REFERENCES

1. S. Pfalzner, *An Introduction to Inertial Confinement Fusion* (Taylor & Francis, New York, 2006).
2. T. J. Murphy, C. W. Barnes, R. R. Berggren, P. Bradley, S. E. Caldwell, R. E. Chrien, J. R. Faulkner, P. L. Gobby, N. M. Hoffman, J. L. Jimerson, K. A. Klare, C. L. Lee, J. M. Mack, G. L. Morgan, J. A. Oertel, F. J. Swenson, P. J. Walsh, R. B. Walton, R. G. Watt, M. D. Wilke, D. C. Wilson, C. S. Young, S. W. Haan, R. A. Lerche, M. J. Moran, T. W. Phillips, T. C. Sangster, R. J. Leeper, C. L. Ruiz, G. W. Cooper, L. Disdier, A. Rouyer, A. Fedotoff, V. Yu. Glebov, D. D. Meyerhofer, J. M. Soares, C. Stockl, J. A. Frenje, D. G. Hicks, C. K. Li, R. D. Petrasso, F. H. Séguin, K. Fletcher, S. Padalino, and R. K. Fisher, *Rev. Sci. Instrum.* **72**, 773 (2001).
3. D. Ress *et al.*, *Science* **241**, 956 (1988).
4. L. Disdier, A. Rouyer, I. Lantuéjoul, O. Landoas, J. L. Bourgade, T. C. Sangster, V. Yu. Glebov, and R. A. Lerche, *Phys. Plasmas* **13**, 056317 (2006).
5. T. R. Boehly, D. L. Brown, R. S. Craxton, R. L. Keck, J. P. Knauer, J. H. Kelly, T. J. Kessler, S. A. Kumpan, S. J. Loucks, S. A. Letzring, F. J. Marshall, R. L. McCrory, S. F. B. Morse, W. Seka, J. M. Soares, and C. P. Verdon, *Opt. Commun.* **133**, 495 (1997).
6. L. Disdier, A. Rouyer, A. Fedotoff, J.-L. Bourgade, F. J. Marshall, V. Yu. Glebov, and C. Stoeckl, *Rev. Sci. Instrum.* **74**, 1832 (2003).
7. M. C. Ghilea, T. C. Sangster, D. D. Meyerhofer, R. A. Lerche, and L. Disdier, *Rev. Sci. Instrum.* **79**, 023501 (2008).
8. R. K. Fisher, R. B. Stephens, L. Disdier, J. L. Bourgade, A. Rouyer, P. A. Jaanimagi, T. C. Sangster, R. A. Lerche, and N. Izumi, *Phys. Plasmas* **9**, 2182 (2002).
9. M. C. Ghilea, D. D. Meyerhofer, and T. C. Sangster, "A Freon-Filled Bubble Chamber for Neutron Detection in Inertial Confinement Fusion Experiments," to be submitted to *Review of Scientific Instruments*.

10. M. C. Ghilea, D. D. Meyerhofer, and T. C. Sangster, "Neutron Detection with Bubble Chambers for Inertial Confinement Fusion on OMEGA," to be submitted to Review of Scientific Instruments.
11. A. Herve *et al.*, Nucl. Instrum. Methods Phys. Res. **202**, 417 (1982).
12. M. Das *et al.*, Radiat. Meas. **30**, 35 (1999).
13. J. W. Gibbs, Connecticut Academy Transactions **3**, 108 (1875-7).
14. L. K. Pan, J. Radioanal. Nucl. Chem. **240**, 707 (1999).
15. C. R. Bell *et al.*, Nucl. Sci. Eng. **53**, 458 (1974).
16. A. Norman and P. Spiegler, Nucl. Sci. Eng. **16**, 213 (1963).
17. C. R. Bell, "Radiation Induced Nucleation of the Vapor Phase," Ph.D. thesis, Massachusetts Institute of Technology, 1970.
18. F. Seitz, Phys. Fluids **1**, 2 (1958).
19. R. E. Apfel and S. C. Roy, Radiat. Prot. Dosim. **10**, 327 (1985).
20. M. Okada *et al.*, J. Chem. Eng. Data **33**, 399 (1988).
21. R. K. Fisher *et al.*, Rev. Sci. Instrum. **72**, 796 (2001).
22. J. Benichou *et al.*, Nucl. Instrum. Methods Phys. Res. **214**, 245 (1983).
23. D. V. Bugg, in *Progress in Nuclear Physics* (Butterworths-Springer, London, 1959), Vol. 7, pp. 1-52.
24. M. S. Plesset and S. A. Zwick, J. Appl. Phys. **25**, 493 (1954).
25. D. Hughes and R. Schwartz, *Neutron Cross Sections*, 2nd. ed (Brookhaven National Laboratory, Upton, NY, 1958).
26. H. A. Bethe and J. Ashkin, in *Experimental Nuclear Physics*, edited by E. Sergrè (Wiley, New York, 1953), Vol. I, pp. 166-357.
27. W. Benenson *et al.*, eds. *Handbook of Physics* (Springer, New York, 2002).
28. M. Dykes *et al.*, Nucl. Instrum. Methods **179**, 487 (1981).
29. H. Tai, *Comparison of Stopping Power and Range Databases for Radiation Transport Study*, NASA Technical Paper (National Aeronautics and Space Administration, Langley Research Center, Hampton, VA, 1997).
30. A. J. Frasca *et al.*, Phys. Rev. **144**, 854 (1966).
31. T. P. Pandya, A. K. Saxena, and B. C. Srivastava, Rev. Sci. Instrum. **47**, 1299 (1976).

